Structural and magnetic properties of $RFe_{10}Mo_2$ and $RFe_{10}Mo_2N$

1996 J. Phys.: Condens. Matter 8 8923

(http://iopscience.iop.org/0953-8984/8/45/024)

J. Phys.: Condens. Matter **8** (1996) 8923–8931. Printed in the UK

Structural and magnetic properties of $RFe_{10}Mo_2$ and $RFe_{10}Mo_2N$

T Zhao†‡, X C Kou§, Z D Zhang†, X K Sun†, Y C Chuang† and F R de Boer‡

† Institute of Metal Research, Academia Sinica, Shenyang 110015, People's Republic of China
‡ van der Waals–Zeeman Laboratory, University of Amsterdam, 1018 XE, Amsterdam, The Netherlands
§ Institut für Experimentalphysik, Technische Universität Wien, Wiedner Hauptstrasse 8-10, A-1040 Wien, Austria

Received 10 January 1996, in final form 2 May 1996

Abstract. The structural and magnetic properties of $RFe_{10}Mo_2$ and $RFe_{10}Mo_2N$ have been studied by x-ray diffraction and high-field magnetization measurements on free-powder or magnetically aligned samples. The lattice of $RFe_{10}Mo_2$ expands anisotropically upon nitrogenation and the volume of the unit cell increases by 2.9–4.0%. The rare-earth element dependence of lattice expansion is found to be just opposite to that of the Curie temperature. The saturation magnetization of $RFe_{10}Mo_2$ increases after the introduction of nitrogen. The abnormally large values of magnetization for some heavy-rare-earth compounds imply that a non-collinear moment configuration in the absence of an external field may exist in these compounds.

1. Introduction

The discovery of the iron-rich ternary phase $Nd_2Fe_{14}B$ gave impetus to the search for iron-rich rare-earth intermetallic compounds for possible application as permanent magnets. Much research work has been concentrated on pseudo-binary $R(Fe_{12-x}M_x)$. Although the RFe_{12} intermetallics do not exist for any rare earth, the $ThMn_{12}$ structure can be stabilized for $x > 1$ and M = Ti, V, Cr, Mo, W, Nb, Al, Ga or Si. [1].

The drastically improved magnetic properties of R_2Fe_{17} compounds by nitrogenation [2] encouraged researchers to introduce nitrogen into $ThMn_{12}$-type iron-rich compounds. These efforts led to the discovery of $R(Fe,T)_{12}N_x$ (T = Ti, V, Si or Mo) compounds [3–10]. The nitrides have the same $ThMn_{12}$ structure, however, with an increase in the unit cell volume by about 4%. The increase in Curie temperature upon nitrogenation ensures that some compounds, such as $Nd(Fe,T)_{12}N_x$ have a T_c suitable for permanent-magnet applications.

In the present paper, the structural and magnetic properties of $RFe_{10}Mo_2$ and $RFe_{10}Mo_2N$ will be investigated in detail.

2. Experimental methods

Polycrystalline $RFe_{10}Mo_2$ ingots with R = Y, Pr, Nd, Gd, Dy, Ho, Er or Tm were prepared by induction melting appropriate amounts of starting materials with a purity of at least 99.99 wt%. The ingots were remelted four times in order to achieve homogeneity. Weight

0953-8984/96/458923+09$19.50

losses during the melting due to evaporation of the rare-earth element were compensated for by starting with an excess of 3 wt% R (with respect to the R content). The as-cast ingots were wrapped in tantalum foil and sealed in a pre-evacuated and then argon-gas-filled quartz tube, followed by annealing at 1373 K for 4 weeks and then water quenching to avoid possible phase transitions during the cooling process. The crystal structures of the samples were checked by means of x-ray diffraction. It was found that all the samples investigated were nearly single phase with the $ThMn_{12}$-type tetragonal structure, except that a small amount of α-Fe was traced as impurity.

The annealed materials were ground to fine powders with a diameter of less that 40 μm to provide enough active surface for the nitrogenation. The nitrogenation was carried out in a quartz ampoule placed in a resistance furnace with a flowing nitrogen atmosphere of purity better than 99.99%. The powder was placed in a quartz container inside the quartz tube. Before nitrogenation, at room temperature, the quartz ampoule with the samples inside was washed by the floating nitrogen gas for about 1 h to remove the air. The nitrides were formed after heat treatment at 500–560 °C for about 10 h. Although the nitride already began to form at a low temperature (500 °C) after a short time (1 h), a longer-time higher-temperature treatment was necessary to obtain homogeneous nitrides. The concentration of nitrogen (number of nitrogen atoms per formula unit) in the nitrides was determined by a weighing method according to the following formula:

$$x_N = \frac{W_1 - W_0}{W_0}\frac{M_0}{M_N} \tag{1}$$

where W_0 and W_1 are the masses of sample before and after nitrogenation, respectively, M_0 is the molecular mass of the compounds and M_N is the atomic mass of nitrogen. The concentration of nitrogen determined by the weighing method is nearly one nitrogen per formula unit for all samples studied, close to the maximum solubility of nitrogen in the 2b site of the $ThMn_{12}$ structure. The crystal structures of nitrides were also analysed by x-ray diffraction.

High-field measurements at 4.2 K were performed on both free-powder and magnetically aligned samples in the high-magnetic-field installation at the van der Waals–Zeeman Laboratory of the University of Amsterdam. In this installation, quasi-static fields up to 40 T can be generated. For high-field free-powder (HFFP) [11, 12] measurements, fine powders (of diameter less than 40 μm) were loaded loosely into the sample holder. These particles can be considered as of a single-crystal nature and are free to rotate in the external field so that the total magnetic moment of samples is always parallel to the external field.

3. Results and discussion

The x-ray diffraction patterns for $YFe_{10}Mo_2$, $YFe_{10}Mo_2N$, $HoFe_{10}Mo_2$ and $HoFe_{10}Mo_2N$ are shown in figures 1 and 2. For accurate determination of the lattice constants, silicon is mixed with the sample as a calibration standard. One can see that the nitrides remain isostructural with the parent compounds; however, all the reflection peaks have shifted significantly to smaller-angle positions. This is due to the lattice expansion upon the introduction of the nitrogen atom into the interstitial sites. After nitrogenation, the (330) peak shifts to a small diffraction angle and just overlaps with the α-Fe peak.

The crystallographic parameters of $RFe_{10}Mo_2$ derived from x-ray pattern are listed in table 1. It can be seen that the unit-cell volume of the compounds with the rare earth varying from Pr to Tm decreases monotonically owing to the lanthanide contraction, but the ratio of the lattice constants remains nearly unchanged.

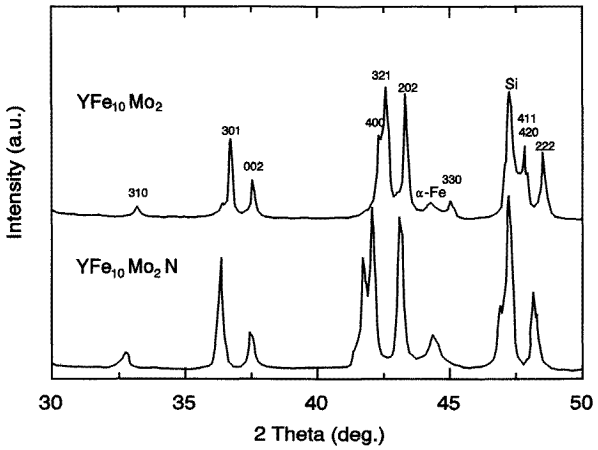

Figure 1. X-ray diffraction patterns of $YFe_{10}Mo_2$ and $YFe_{10}Mo_2N$.

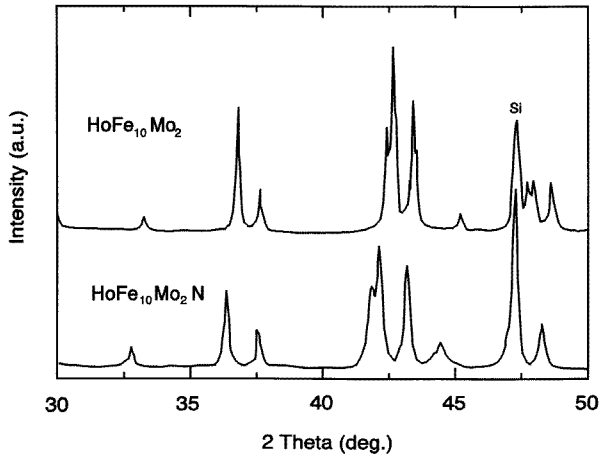

Figure 2. X-ray diffraction patterns of $HoFe_{10}Mo_2$ and $HoFe_{10}Mo_2N$.

The lattice parameters of $RFe_{10}Mo_2N$ as well as the resulting volume expansion in nitrides are also listed in table 1. The c/a ratios of $RFe_{10}Mo_2$ except for R = Pr and R = Nd decrease upon nitrogenation, suggesting that the lattice expansion is mainly along the (a, b) plane. This anisotropic expansion is a common feature of the 1:12 interstitial compounds for both Ti and Mo systems containing N and C [7]. According to neutron diffraction, the nitrogen is located at the 2b site [8, 9]. The 2b site is the largest interstitial site in $RFe_{10}Mo_2$, which is between two 2a rare-earth atoms along the c axis and surrounded by four 8j Fe atoms in the (a, b) plane. Assuming that $r_{Fe} = d_{8i-8i}/2$ and $r_R = d_{2a-8j} - r_{Fe}$ where d_{8i-8i} and d_{2a-8j} are the shortest distances between Fe and Fe atoms and between R and Fe atoms, respectively, and r_R and r_{Fe} are the radii of R and Fe atoms, respectively, we can determine the vacancy size from $r_{2a-2a} = d_{2a-2a} - 2r_R$ and $r_{8j-8j} = d_{8j-8j} - 2r_{Fe}$. Using the neutron diffraction data [9] and the lattice constants given in table 1, the calculated r_{2a-2a} and r_{8j-8j} for $YFe_{10}Mo_2$ are 1.06 Å and 1.41 Å, respectively. If we consider the nitrogen atom as

Table 1. Structural parameters of $RFe_{10}Mo_2$ and $RFe_{10}Mo_2N$.

Compound	a (Å)	c (Å)	V (Å^3)	c/a	$\Delta V/V$ (%)
$YFe_{10}Mo_2$	8.5204	4.7772	346.81	0.561	—
$YFe_{10}Mo_2N$	8.6390	4.7871	357.25	0.554	3.01
$PrFe_{10}Mo_2$	8.5931	4.7896	353.67	0.557	—
$PrFe_{10}Mo_2N$	8.6671	4.8655	365.48	0.561	3.34
$NdFe_{10}Mo_2$	8.5843	4.7867	352.73	0.558	—
$NdFe_{10}Mo_2N$	8.6582	4.8580	363.56	0.562	3.07
$GdFe_{10}Mo_2$	8.5474	4.7818	349.35	0.559	—
$GdFe_{10}Mo_2N$	8.6390	4.8173	359.52	0.558	2.91
$DyFe_{10}Mo_2$	8.5272	4.7808	347.63	0.561	—
$DyFe_{10}Mo_2N$	8.6494	4.7928	358.10	0.554	3.09
$HoFe_{10}Mo_2$	8.5077	4.7713	345.35	0.561	—
$HoFe_{10}Mo_2N$	8.6326	4.7821	356.37	0.554	3.19
$ErFe_{10}Mo_2$	8.5008	4.7682	344.57	0.561	—
$ErFe_{10}Mo_2N$	8.6312	4.7787	355.78	0.553	3.25
$TmFe_{10}Mo_2$	8.4837	4.7634	342.83	0.561	—
$TmFe_{10}Mo_2N$	8.6430	4.7730	356.55	0.552	4.00

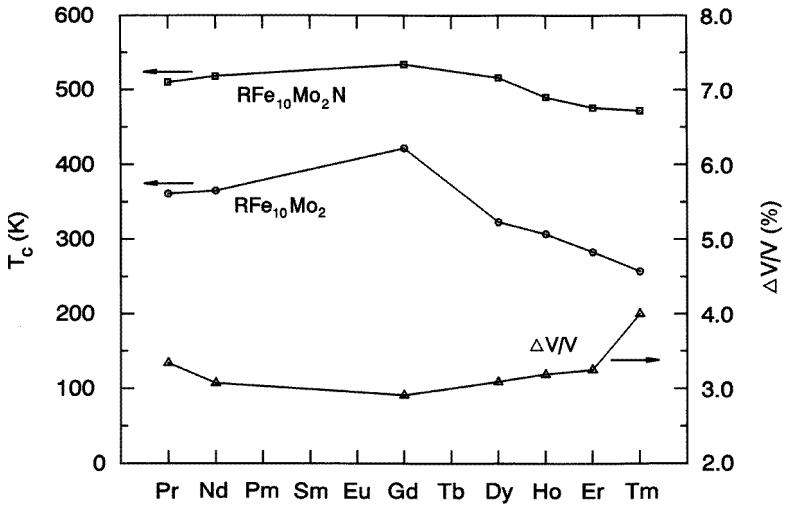

Figure 3. Rare-earth element dependence of Curie temperatures of the $RFe_{10}Mo_2$ compounds before and after nitrogenation and volume expansion upon nitrogenation.

a hard sphere, the lattice will expand mainly along the c axis, which does not agree with the experimental observation. In addition, the lattice expansion would be much larger than experimental data. The experimentally found anisotropic expansion might be due to the strong hybridization of the rare-earth 5d-electron states and the nitrogen 2p-electron states and relatively weak hybridization of transition-metal 3d states. It is interesting to note that, unlike the anisotropic expansion in heavy-rare-earth compounds, the lattice expansion in light-rare-earth compounds (R = Pr, Nd or Sm) upon nitrogenation is nearly isotropic (see table 1 and also [3]). Since the main difference between light- and heavy-rare-earth elements comes from the 4f-electron states, this phenomenon implies participation of 4f-electron states into the hybridization of the rare-earth and nitrogen electron states. The 4f-electron states

Table 2. Magnetic properties of $RFe_{10}Mo_2$ and $RFe_{10}Mo_2N$.

Compound	M_R (μ_B/FU)	M_s (μ_B/FU)	M_{Fe} (μ_B/FU)	α_{RT} (deg)	T_c (K)
$YFe_{10}Mo_2$	0	14.06	14.06	—	309
$YFe_{10}Mo_2N$	0	16.70	16.70	—	485
$PrFe_{10}Mo_2$	3.20	17.65	14.45	—	361
$PrFe_{10}Mo_2N$	3.20	18.71	15.51	—	510
$NdFe_{10}Mo_2$	3.27	18.22	14.95	—	365
$NdFe_{10}Mo_2N$	3.27	18.30	15.03	—	518
$GdFe_{10}Mo_2$	7	6.12	13.12	—	422
$GdFe_{10}Mo_2N$	7	14.30	21.30	122	534
$DyFe_{10}Mo_2$	10	5.52	15.52	—	323
$DyFe_{10}Mo_2N$	10	7.22	17.22	168	516
$HoFe_{10}Mo_2$	10	5.01	15.01	—	307
$HoFe_{10}Mo_2N$	10	11.92	21.92	135	490
$ErFe_{10}Mo_2$	9	6.18	15.18	—	286
$ErFe_{10}Mo_2N$	9	13.92	22.92	135	476
$TmFe_{10}Mo_2$	7	7.22	14.22	—	257
$TmFe_{10}Mo_2N$	7	7.57	14.57	—	472

of the rare-earth elements may play an important role in the lattice expansion of $RFe_{10}Mo_2$ upon nitrogenation.

Upon nitrogenation, the unit-cell volume of $RFe_{10}Mo_2$ compounds expands by 2.9–4.0% which is nearly half the lattice expansion observed for $R_2Fe_{17}N_x$ compounds. The values of lattice expansion are in good agreement with those given in [3, 4, 6, 7]. One can see from table 1 that the lattice expansion has a minimum for $GdFe_{10}Mo_2N$. Maximum expansion was detected for $TmFe_{10}Mo_2N$. This behaviour is opposite to the R dependence of the Curie temperatures of the $RFe_{10}Mo_2$ compounds (figure 3). In other words, the parent compound with the highest Curie temperature has the smallest lattice expansion after nitrogenation. The strongly peaked shape of the R dependence of the Curie temperature is due to the maximum value of $(g_J - 1)[J_R(J_R + 1)]^{1/2}$ for the gadolinium ion which has a half-filled 4f-shell and does not possess an orbital angular momentum. The moderation of the peaked shape of the R dependence of the Curie temperature after nitrogenation (see figure 3) implies a relative decrease in the R–T exchange interaction upon nitrogenation. However, the R dependence of lattice expansion for $RFe_{10}Mo_2N$ might be attributed to the effect of the angular distribution of the 4f-electron density on the hybridization between the rare-earth electron states and the nitrogen electron states. To interpret this phenomenon clearly, further experiments or first-principle calculations on the electronic structures are needed.

To obtain information on saturation magnetization and the exchange interaction, HFFP measurements at 4.2 K have been performed on all $RFe_{10}Mo_2$ and $RFe_{10}Mo_2N$ compounds. The values of the saturation magnetization M_s, obtained by extrapolation of the low-field parts of the magnetic isotherms are given in table 2.

In $YFe_{10}Mo_2$ and $YFe_{10}Mo_2N$ where Y is non-magnetic, the mean Fe moment can be directly deduced from the saturation magnetization. For $YFe_{10}Mo_2N$, the mean Fe moment is $1.67\mu_B$ which is between the value of $1.62\mu_B$ obtained by Anagnostou *et al* [3] and the value of $1.74\mu_B$ found by Hong Sun *et al* [7]. After nitrogenation, the mean magnetic moment of Fe increases by $0.26\mu_B$. The nitrogen introduction usually leads to a twofold influence on the Fe moment: firstly the moment increases by narrowing of the 3d band as a result of the lattice expansion, and secondly the moment decreases by hybridization of the

N 2p-electron state and the Fe 3d-electron states at Fe sites close to the nitrogen. The net effect of nitrogenation is a slight increase in the average Fe moment. From x-ray diffraction on magnetically aligned powder, it follows that the easy-magnetization direction (EMD) of $YFe_{10}Mo_2$ is the *c* axis, whereas the easy direction of $YFe_{10}Mo_2N$ lies in a cone. This can be attributed to the effect of the anisotropic lattice expansion, caused by nitrogenation, on the crystalline electric field.

In the Nd and Pr compounds, assuming the magnetic moment of the rare-earth ion to be parallel to the moment of the Fe sublattice, the Fe moment (see table 2) can be deduced by subtracting the free-ion rare-earth moment from the saturation magnetization. Usually, strong hysteresis will not occur in the free-powder magnetization process because the fine single-crystal particles are free to rotate in the external magnetic field. However, significant hysteresis loops were found in the free-powder magnetization processes in $PrFe_{10}Mo_2N$ (figure 4) and $NdFe_{10}Mo_2N$. The fine particles may or may not be of a single-crystal nature. If they are, these phenomena might be attributed to special domain processes or interactions between the magnetic particles. If a high anisotropy energy exists relative to the exchange energy, the domain wall would be fairly narrow and could give rise to a hysteretic behaviour. In order to obtain information about the anistotropy, magnetic measurements at 4.2 K are performed on magnetically aligned $NdFe_{10}Mo_2N$ and $PrFe_{10}Mo_2N$ samples with an external field parallel or perpendicular to the alignment axis (figure 5). The anisotropy fields of these two nitrides, estimated from intersections of the high-field part of the magnetization curves with the external field parallel and perpendicular to the alignment direction, are very large (greater than 30 T). In $NdFe_{10}Mo_2$, a spin reorientation (SR) from the *c* axis at high temperatures to a cone at low temperatures was found at 147 K by Kou *et al* [13]. However, no trace of SR is detectable in $NdFe_{10}Mo_2N$ by measuring the temperature dependence of AC susceptibility in the temperature range from 4.2 to 800 K. The easy-magnetization direction of $NdFe_{10}Mo_2N$ lies parallel to the *c* axis over the whole magnetic ordering temperature range (from 4.2 K to the Curie temperature) [6, 10]. The magnetic anisotropy of $NdFe_{10}Mo_2N$ originates from two contributions, namely Nd- and Fe-sublattice anisotropies. The strong uniaxial anisotropy detected in $NdFe_{10}Mo_2N$ indicates that the Nd-sublattice anisotropy favours the *c* axis since the Fe-sublattice anisotropy favours a cone according to the data on $YFe_{10}Mo_2N$. It is also found that the EMD of $PrFe_{10}Mo_2N$ is the *c* axis over the whole magnetic ordering temperature range.

In the heavy-rare-earth compounds, the moments of the rare-earth ions are usually coupled antiparallel to the moments of the transition-metal ions. In the $RFe_{10}Mo_2$ compounds, the total Fe moment is larger than that of the rare-earth ions. Therefore, the Fe moment can be estimated by adding the experimentally obtained saturation magnetization to the free-ion moment of the corresponding rare-earth ion. The Fe moments obtained for $RFe_{10}Mo_2$ compounds are in the range $(1.31–1.55)\mu_B$. However, for the nitrides the derived Fe moments vary from $1.46\mu_B$ for the Tm compound to $2.29\mu_B$ for the Er compound. Such anomalously large values for the Fe moment are also found for Ho and Gd compounds. At first glance, one may attribute the large Fe moments to the existence of a certain amount of α-Fe as the impurity phase, but if we take the value $1.67\mu_B$ for $YFe_{10}Mo_2N$ as a reasonable value, there should be more than 20% α-Fe as impurity phase in these compounds. From the x-ray diffraction pattern of $HoFe_{10}Mo_2N$, in which the relative intensity of the α-Fe + (330) peak is comparable with that in $YFe_{10}Mo_2$, one can conclude that there is not this much α-Fe in the sample. Another possibility is that the moments of the Fe sublattice and the rare-earth sublattice are not aligned collinearly because of competition between anisotropies of these two sublattices, and this may lead to a much larger M_s compared with that of the antiparallel configuration of sublattice moments. In this case, if we use $1.67\mu_B$ as the Fe

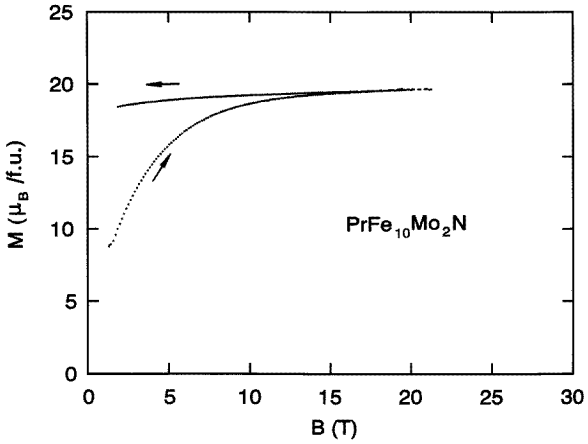

Figure 4. Magnetic isotherms at 4.2 K of $PrFe_{10}Mo_2N$ measured on powder particles that are free to rotate in the sample holder.

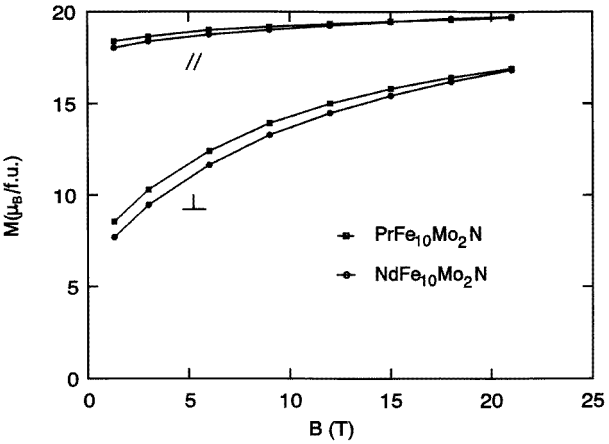

Figure 5. Magnetic isotherms at 4.2 K of $PrFe_{10}Mo_2N$ and $NdFe_{10}Mo_2N$ measured on a magnetically aligned sample with the external field parallel or perpendicular to the alignment axis.

moment M_T and the free-ion value for rare-earth moment M_R, we may derive the angle α_{RT} between the moments of the Fe sublattice and the rare-earth sublattice (see table 2). The values of α_{RT} are obtained from the following formula:

$$\alpha_{RT} = \cos^{-1}\left(\frac{M_s^2 - M_T^2 - M_R^2}{2M_T M_R}\right). \tag{2}$$

This picture is no longer valid for $GdFe_{10}Mo_2$ as the Gd ion must be regarded as an isotropic s-state ion. However, the strong hybridization of the rare-earth 5d-electron states and the nitrogen s-electron states along the c axis may induce anisotropy in the Gd ion. This assumption indicates a decrease in the intersublattice exchange interaction between the Fe and the rare-earth moments upon nitrogenation. The third possibility is that the interior 4f-electron state is also affected by the strong hybridization of the rare-earth and nitrogen

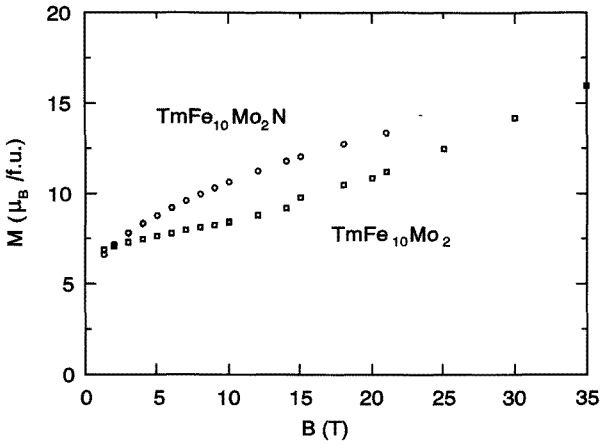

Figure 6. Magnetic isotherms at 4.2 K of $TmFe_{10}Mo_2$ and $TmFe_{10}Mo_2N$ measured on powder particles that are free to rotate in the sample holder.

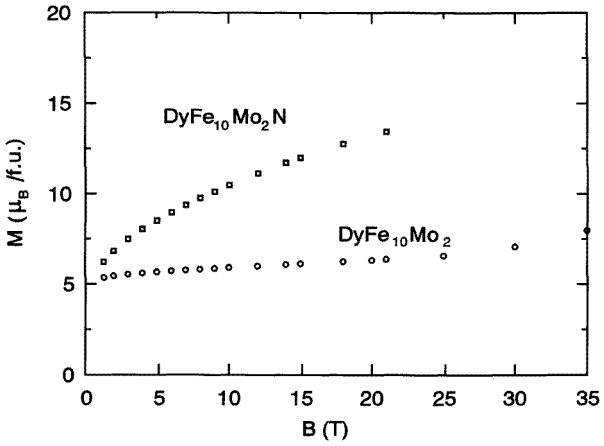

Figure 7. Magnetic isotherms at 4.2 K of $DyFe_{10}Mo_2$ and $DyFe_{10}Mo_2N$ measured on powder particles that are free to rotate in the sample holder.

electron state and the magnetic moment of the R-sublattice decreases upon nitrogenation. The strong anisotropic lattice expansion upon nitrogenation supports the last assumption.

For $TmFe_{10}Mo_2$ (figure 6) and $DyFe_{10}Mo_2$ (figure 7), the magnetic moment of Fe changes only slightly upon nitrogenation. The flat section in the low-field magnetization of the parent compounds, corresponding to the collinear configuration of Fe and rare-earth moments, has disappeared. Instead, a section with a large slope, which may correspond to a bending process, starts already from zero field. This is one of the characteristics of a system with a non-collinear configuration at zero field [14], which is the result of competition between anisotropies of the magnetic sublattices and also implies a relatively weak exchange interaction. Since high-order anisotropy terms are found to be very large in some of the 1:12 compounds [15], they might also play an important role in inducing a non-collinear configuration [14]. This result is similar to that observed in $R_2Co_{17}N_x$ [16]

and suggests that the nitrogenation leads to a decreases of the R–T exchange interaction in the R–T compounds.

4. Conclusion

Both the $RFe_{10}Mo_2$ compounds and their nitrides investigated possess the tetragonal $ThMn_{12}$ type of structure. The lattice expands anisotropically upon nitrogenation. Very large anisotropies are obtained in the compounds $PrFe_{10}Mo_2N$ and $NdFe_{10}Mo_2N$ and give rise to hysteretic behaviour during the free-powder magnetization processes of these compounds. The high-field free-powder measurements on the heavy-rare-earth compounds suggest that the intersublattice exchange interaction between the Fe and the rare-earth moments decreases with introduction of interstitial nitrogen atoms and that a non-collinear configuration between the rare-earth and the Fe moments may exist at zero external field.

Acknowledgments

This work has been supported by the exchange programme between China and the Netherlands, the National Natural Sciences Foundation of China, the Sciences and Technology Commission of Shenyang, and the President Foundation of the Chinese Academy of Science.

References

[1] Li H S and Coey J M D 1991 *Magnetic Materials* vol 6, ed K H J Buschow (Amsterdam: North-Holland) ch 1
[2] Coey J M D and Hong Sun 1990 *J. Magn. Magn. Mater.* **87** L251
[3] Anagnostou M, Christides C and Niarchos D 1991 *Solid State Commun.* **78** 681
[4] Anagnostou M, Christides C, Pissas M and Niarchos D 1991 *J. Appl. Phys.* **70** 6012
[5] Chen X, Liao L X, Altounian Z, Ryan D H and Ström-Olsen J O 1992 *J. Magn. Magn. Mater.* **111** 130
[6] Tomey E, Isnard O, Fagan A, Desmoulins C, Miraglia S, Soubeyroux J L and Fruchart D 1993 *J. Alloys Comp.* **191** 233
[7] Hong Sun, Akayama M, Tatami K and Fujii H 1993 *Physica* B **183** 33
[8] Wang Y Z, Hadjipanayis G C, Tang Z X, Yelon W B, Papaefthymiou V, Moukarika A and Sellmyer D J 1993 *J. Magn. Magn. Mater.* **119** 41
[9] Ishida S, Asano S and Fujii S 1994 *Physica* B **193** 66
[10] Sinnecker E H C P, Kou X C and Grössinger R 1995 *IEEE Trans. Magn.* **31** 3707
[11] Verhoef R, de Boer F R, Franse J J M, Dennisen C J M, Jacobs T H and Buschow K H J 1989 *J. Magn. Magn. Mater.* **80** 41
[12] Verhoef R, Radwanski R J and Franse J J M 1990 *J. Magn. Magn. Mater.* **81** 176
[13] Kou X C, Grössinger R, Wiesinger G, Liu J P, de Boer F R, Kleinschroth I and Kronmüller H 1995 *Phys. Rev.* B **51** 8254
[14] Zhang Z D, Zhao T, de Chatel P and de Boer F R 1995 *J. Magn. Magn. Mater.* **147** 74
[15] Hurley D P F, Kuzmin M, Coey J M D and Kohgi M 1995 *J. Magn. Magn. Mater.* **140–144** 1027
[16] Liu J P, Zhang Z D, Zeng D C, Tang N, de Chatel P F and de Boer F R 1994 *IEEE Trans. Magn.* **30** 613